Progress In Electromagnetics Research B, Vol. 45, 309–335, 2012

OBLIQUE INCIDENCE DESIGN OF MEANDER-LINE POLARIZERS FOR DIELECTRIC LENS ANTENNAS

M. Letizia*, B. Fuchs, C. Zorraquino, J. F. Zürcher, and J. R. Mosig

Laboratory of Electromagnetics and Acoustics (LEMA), Ecole Polytechnique Fédérale de Lausanne (EPFL), EPFL Station 11, Lausanne CH-1015, Switzerland

Abstract—A method to design planar multilayer meander-line polarizers is given. The proposed procedure is based on transmission line circuit theory and on full-wave unit cell analysis in frequency domain. The hybrid combination of those two techniques paves the way for the polarizer design process and avoids heavy full-wave optimizations. This procedure is originally aimed for polarizers acting on lens antennas and is suitable for plane waves impinging with arbitrary angles on the polarizer. To validate the proposed method, two polarizers have been manufactured in Ka-band, one for normal and one for oblique incidence. Designs, prototypes and measurements made on a complete Ka-band lens antenna subsystem are shown in this paper.

1. INTRODUCTION

Many communication systems require the use of high gain circularly polarized multi-beam antennas. Typical examples are radar systems [1, 2], geostationary satellites [3] and High Altitude Platform Stations (HAPS) [4]. Multiple beams allow switching between different antenna footprints while increasing the capacity of the communication channel [5]. On the other hand, circular polarization is the standard solution to overcome misalignments between transmitter and receiver and to mitigate the multipath problems.

From the frequency point of view, the migration towards higher frequencies, providing larger bandwidths and hence channel capacities, is a continuous trend. Nowadays, the Ka-band (around 30 GHz)

Received 8 August 2012, Accepted 11 October 2012, Scheduled 1 November 2012
* Corresponding author: Marco Letizia (marco.letizia@epfl.ch).

is considered as very promising for this type of applications and, probably, one of the most useful implementations at this frequency is the use of a dielectric lens fed by several feeds [6]. In this type of antenna system, the circular polarization (CP) can be obtained essentially in two ways: either the elementary radiators feeding the lens are already circularly polarized or they are linearly polarized and CP is generated after the lens with the help of an external polarizer.

A preliminary comparison between both systems [7] has shown that the lens might considerably degrade the quality of a CP source. On the other hand, an external polarizer can easily provide a better solution when it is placed normally respect to the incident wave. But, again, CP quality will degrade for oblique incidence, which is an expected occurrence in usual operating mode of these antenna systems. In this paper, we present a design approach for planar multilayered printed polarizers, intended to generate CP from a linearly polarized incident wave coming from a dielectric lens and impinging the polarizer at, possibly, an oblique angle.

Multilayered planar polarizers are convenient devices to transform the fields of a linearly polarized antenna into a circularly polarized wave at millimeter-wave frequencies [8]. A typical polarizer can be made of several stacked printed-meander-line sheets (the "grating" layer) separated by dielectric spacers. The principle of operation of this meander-line (ML) polarizer is well known [9] and results from the different action of the grating on the two orthogonal components of the incident field.

One of the useful characteristics of this type of polarizer is its independence from the antenna properties. Indeed, the polarizer may be thought as an add-on that does not affect the performance parameters of the antenna [10].

The ML polarizer has been proposed in [9] and improved in [11]. Later, [12–15] gave analytical formulas to compute the phase delay and characterize the polarizer's grating layer. Transmission line theory together with Method of Moments based algorithms has been used by [13, 16–18] to analyze the ML polarizer.

All these contributions were primarily focused on polarizers which are supposed to work with normally incident plane waves. However, it is clear from literature results [10, 16, 19, 20] that the performances of this type of polarizers gradually deteriorate for higher angles of incidence. This represents a limitation for multi-beam antenna system in which oblique incidence is a ubiquitous situation.

In this paper, we propose a method to design a planar ML polarizer suitable for oblique incidence. This polarizer is intended to work as a component of an antenna subsystem including a dielectric

lens antenna and Ka-band circular horns used as primary radiators. The paper concentrates on the polarizer design since the other elements (elementary radiator, lens) have been described elsewhere [6]. However, the polarizer performances are indirectly characterized through measurements of the global subsystem performances which, at the end of the day, are the ones of practical interest. The proposed method follows closely the approach discussed in [16], avoids the use of full wave analysis to characterize the entire polarizer and it is based on the combination of transmission line (TL) model and unit cell full wave analysis with periodic boundaries conditions. As a proof of concept, two prototypes are designed following the proposed procedure, built and measured. The first prototype is designed for normal incidence, whereas a second prototype is optimized for oblique incidence ($\theta_{inc} = 25°$, i.e., the direction of propagation of the incident wave is 25° with respect to the normal of the polarizer surface).

After a presentation of the polarizer's working principle in Section 2, the method used to design the polarizer is explained in Section 3. Section 4 shows the synthesized performances of the optimized polarizers. The optimal working condition of the TL model is perturbed by including the effect of non-idealities (i.e., mechanical tolerances) in the model. This sensitivity analysis is presented in Section 5 whereas the performances of two prototypes are shown in Section 6. Finally, Section 7 concludes and summarizes the paper.

2. MEANDER-LINE (ML) POLARIZER

2.1. Working Principle

The ML polarizer is a multilayer structure composed of different sections (Fig. 1). Each section is made by conducting meander lines which are etched on a dielectric substrate and separated by dielectric spacers.

Figure 2 depicts the geometry considered here. The z-axis is defined as normal to the polarizer surface. For the sake of simplicity, we define the x-axis in such a way that the wave vector $\mathbf{k_{inc}}$ of the incident wave is located in the xz-plane. Thus, the angle of incidence θ_{inc} is customarily defined in the xz-plane as the angle between $\mathbf{k_{inc}}$ and the z-axis.

We consider now an incident wave generating an electric field $\mathbf{E_{inc}}$ along the y-axis (Fig. 2) and we place the metallizations in the xy-plane in such a way that the meanders' axes are all oriented at an angle Ψ respect to the incident electric field. Ψ is known as the "polarizer orientation angle".

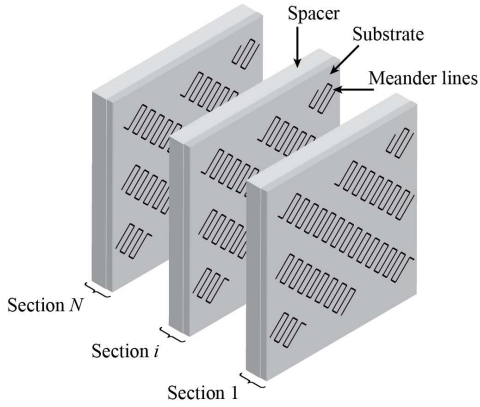

Figure 1. Meander line (ML) polarizer geometry. The polarizer is composed by N sections. For each section, the meander-line gratings are printed on dielectric substrate. The spacer separates the gratings of different sections.

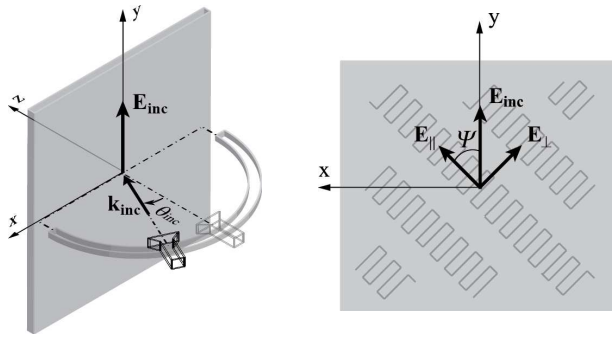

(a) (b)

Figure 2. Coordinate system. (a) θ_{inc} defines the direction of arrival of the incident wave and $\mathbf{k_{inc}}$ its pointing vector. (b) The polarizer grating and the electric field $\mathbf{E_{inc}}$ belong to the x-y plane. Ψ defines the angle between the meander-line axis and $\mathbf{E_{inc}}$ on the x-y plane.

The incident electric field can now be decomposed into components parallel to the meanders' axis and perpendicular to it, respectively $\mathbf{E}_{||}$ and $\mathbf{E}_{\perp}$:

$$\mathbf{E_{inc}} = \mathbf{E}_{||} + \mathbf{E}_{\perp} = |\mathbf{E_{inc}}| \cos\Psi \hat{\mathbf{e}}_{||} + |\mathbf{E_{inc}}| \sin\Psi \hat{\mathbf{e}}_{\perp} \qquad (1)$$

In a typical ML polarizers operation the polarizer's orientation angle takes the value $\Psi = 45°$, thus resulting in identical values for the components $\mathbf{E}_{||}$ and $\mathbf{E}_{\perp}$.

As it is well known [19], a CP wave can be obtained by designing a meander-line polarizer that introduces a differential phase shift of 90° between the components $\mathbf{E}_{||}$ and $\mathbf{E}_{\perp}$ while keeping their amplitudes identical. A proper design will also ensure a reasonable CP axial ratio over a broad frequency bandwidth and for a wide range of incident angles [19]. Right-hand or left-hand circular polarizations can be easily obtained selecting the sign of the polarizer orientation angle Ψ ($\pm 45°$).

2.2. Transmission Line Model

The ML polarizer reacts differently to the parallel and horizontal components of the incident field, thus it is electrically treated as a four-port device (see Fig. 3) with respect to these components. The grating is seen by $\mathbf{E}_{||}$ and $\mathbf{E}_{\perp}$ as, respectively, an inductive and a capacitive load [21]. Therefore, shunt admittances ($1/j\omega L_{eq}$ and $j\omega C_{eq}$) are chosen to model the grating for the two components of $\mathbf{E_{inc}}$ and transmission lines are used to model the dielectric materials between different gratings.

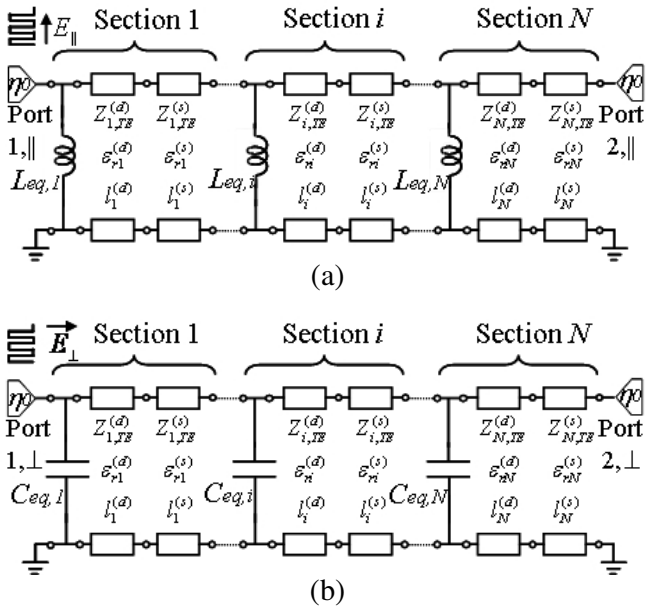

Figure 3. Transmission line model of the meander-line polarizer. (a) For the parallel component of the incident electric field and (b) for the perpendicular component of the incident electric field.

This is clearly depicted in the multiport transmission line model of Fig. 3, where the reference impedance for both the input and output ports is the free-space impedance $\eta_0 = 377\,\Omega$. The transmission line lengths $l^{(s)}$ and $l^{(d)}$ correspond, respectively, to the thicknesses of the spacer and of the dielectric. Snell's law is used to compute the angle of incidence of the propagating wave in each section i of the polarizer both for the spacer (characterized by a relative permittivity $\epsilon_{r,i}^{(s)}$) and for the dielectric substrate (characterized by a relative permittivity $\epsilon_{r,i}^{(s)}$):

$$\sqrt{\epsilon_{r,i}^{(s)}}\sin\theta_{inc,i}^{(s)} = \sqrt{\epsilon_{r,i}^{(d)}}\sin\theta_{inc,i}^{(d)} = \sin\theta_{inc} \tag{2}$$

Since the incident field is always parallel to the dielectric surfaces of the polarizer (in all the sections and for any θ_{inc}), the propagation constants of transmission lines are given by [22]:

$$\beta_i^{(m)} = \frac{2\pi f_0\sqrt{\epsilon_{r,i}^{(m)}}}{c}\cos\theta_{inc,i}^{(d)}, \quad \text{for } m = \{s, d\} \tag{3}$$

where $m = s$ and $m = d$ indicate, respectively, the spacer and the dielectric substrate.

3. POLARIZER DESIGN PROCEDURE

The design procedure aims to find the optimized dimensions of the polarizer. The approach for the solution of the problem is described in the flow-chart of Fig. 4. We first include the design input parameters (i.e., f_0, θ_{inc}, dielectric materials ...) in the TL model. Then we solve this model to find the shunt components $L_{eq,i}$ and $C_{eq,i}$ which are not directly related to the input specification parameters of the polarizer. Once the TL model is properly characterized, the dimensions of the meander are optimized, for each layer, using a full-wave unit cell analysis.

3.1. Specifications and Analyzed Parameters (Input Parameters)

The design procedure starts by considering the relevant specifications and the input parameters that remain invariant during the polarizer design process:

- the center frequency f_0 ;
- the angle of incidence θ_{inc};

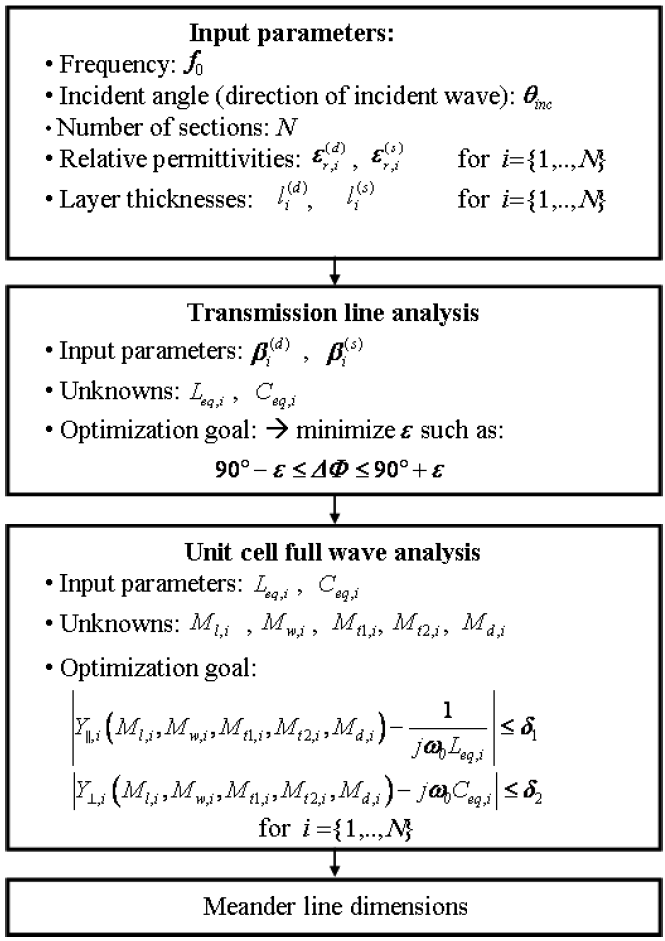

Figure 4. Flow chart of the meander-line polarizer design procedure.

- the number of sections N of the polarizer;
- the relative permittivity and the thickness of the dielectric materials.

For the sake of clarity and without loss of generality, we consider a polarizer with $N = 4$ sections, working at the central frequency $f_0 = 29\,\text{GHz}$ and oriented at the nominal angle $\Psi = 45°$. Since the angle Ψ and the substrate quantities are fixed before designing the polarizer, the phase shift between the components $\mathbf{E}_{||}$ and $\mathbf{E}_{\perp}$ after crossing the polarizer is the parameter that plays the most important role in controlling the polarizer optimization.

3.2. The Transmission Line Analysis

The goal of the transmission line analysis is to characterize the phase shift accumulated by $\mathbf{E}_{||}$ and $\mathbf{E}_{\perp}$ during the propagation through the different sections of the polarizer, as well as their eventual amplitude mismatch.

T-matrix formulation is used to analyze the multilayered meander line structures. Each element of the two equivalent circuits is associated to its **T**-matrix. The **T**-matrix of the transmission lines of the i-th section is given by [22]:

$$\mathbf{T}_i^{(m)} = \begin{bmatrix} \cos\left(\beta_i^{(m)} l_i^{(m)}\right) & j\frac{\eta_0 \cos\theta_{inc,i}^{(m)}}{\sqrt{\epsilon_{r,i}^{(m)}}} \sin\left(\beta_i^{(m)} l_i^{(m)}\right) \\ j\frac{\sqrt{\epsilon_{r,i}^{(m)}}}{\eta_0 \cos\theta_{inc,i}^{(m)}} \sin\left(\beta_i^{(m)} l_i^{(m)}\right) & \cos\left(\beta_i^{(m)} l_i^{(m)}\right) \end{bmatrix} \quad (4)$$

for $m = s,\ d$.

The transmission matrices $\mathbf{T}_i^{\mathrm{L}}$ and $\mathbf{T}_i^{\mathrm{C}}$ of the shunt components of the i-th section are obviously given by:

$$\mathbf{T}_i^{\mathrm{L}} = \begin{bmatrix} 1 & 0 \\ \frac{1}{j\omega L_{eq,i}} & 1 \end{bmatrix} \quad (5)$$

$$\mathbf{T}_i^{\mathrm{C}} = \begin{bmatrix} 1 & 0 \\ j\omega C_{eq,i} & 1 \end{bmatrix} \quad (6)$$

By cascading the transmission matrices of each section of the equivalent circuit, we obtain the transmission matrices $\mathbf{T}_{||}$ and $\mathbf{T}_{\perp}$ associated to the vertical and horizontal component respectively:

$$\mathbf{T}_{||} = \prod_{i=1}^{N=4} \mathbf{T}_i^{\mathrm{L}} \mathbf{T}_i^{\mathrm{d}} \mathbf{T}_i^{\mathrm{s}} \quad (7)$$

$$\mathbf{T}_{\perp} = \prod_{i=1}^{N=4} \mathbf{T}_i^{\mathrm{C}} \mathbf{T}_i^{\mathrm{d}} \mathbf{T}_i^{\mathrm{s}} \quad (8)$$

From these two analyses, we compute the scattering transmission parameters, $S_{21,||}$ and $S_{21,\perp}$, as explained in [22]. The differential phase shift $\Delta\Phi$ is computed as $\Delta\Phi = \angle S_{21,\perp} - \angle S_{21,||}$ whereas the magnitude difference ΔM is computed as $\Delta M = |S_{21,\perp}| - |S_{21,||}|$.

In this model, the shunt elements are optimized using quasi-Newton algorithm in order to obtain a differential phase shift $\Delta\Phi$ as close as possible to 90°.

As a final step, the AR performance of the polarizer is estimated by using transmission line theory [23] as:

$$\mathrm{AR} = \left(\frac{\left|S_{21,||}\right|^2 + \left|S_{21,\perp}\right|^2 + \sqrt{a}}{\left|S_{21,||}\right|^2 + \left|S_{21,\perp}\right|^2 - \sqrt{a}} \right)^{\frac{1}{2}} \tag{9}$$

where $a = \left|S_{21,||}\right|^4 + \left|S_{21,\perp}\right|^4 + 2\left|S_{21,||}\right|^2 \left|S_{21,\perp}\right|^2 \cos\left(2\Delta\Phi\right)$.

3.3. The Unit Cell Full Wave Analysis

The full-wave analysis of the unit cell aims to provide the physical dimensions of the meander-lines. Fig. 5 shows in detail the geometry of a single meander section. M_l is the meander section length and M_w the meander section width. The meander line shows two different widths M_{t1} and M_{t2} and M_d is the distance between adjacent meander-line axes. Due to the periodicity of the meander lines, the gratings are modeled by imposing periodic boundary conditions on the unit cell. This is easily implemented in modern FEM software [24]. The unit cell (Fig. 5) accommodates only one meander of the i-th layer. The electromagnetic source is modeled as a linearly polarized plane wave impinging on the meander inside the unit cell. The direction of the excitation is $\theta_{inc,i}$ (different for each layer according to the computed transmission line analysis). The unit cell is analyzed separately for the two components $\mathbf{E}_{||}$ and $\mathbf{E}_{\perp}$ and the admittances $Y_{||,i}$ and $Y_{\perp,i}$ are respectively computed. Both analyses need to be performed for the N sections of the polarizer.

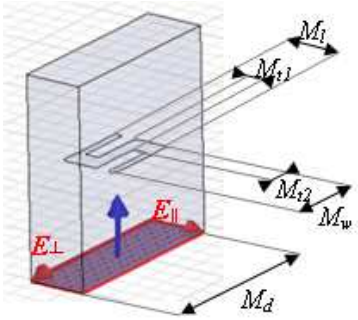

Figure 5. Meander model used for the unit cell analysis. The parallel component ($\mathbf{E}_{||}$) excites the structure (The excitation is oriented along the meander line axis). The perpendicular component ($\mathbf{E}_{\perp}$) excites the structure (The excitation is normal to the meander line axis).

The meander dimensions (M_l, M_w, M_{t1}, M_{t2}, M_d) are adjusted until the admittances $Y_{||,i}$ and $Y_{\perp,i}$ are close the values ($j\omega_0 C_{eq}$ and $1/j\omega_0 L_{eq}$) found in the equivalent circuit analysis. A quasi-Newton algorithm is used for the minimization of the absolute values of the differences between the numerically found admittances and their lumped-element counterparts until they pass below some threshold values δ_1 and δ_2:

$$\left| Y_{||,i}\left(M_{l,i}, M_{w,i}, M_{t1,i}, M_{t2,i}, M_{d,i}\right) - \frac{1}{j\omega_0 L_{eq,i}} \right| \leq \delta_1 \tag{10}$$

$$\left| Y_{\perp,i}\left(M_{l,i}, M_{w,i}, M_{t1,i}, M_{t2,i}, M_{d,i}\right) - j\omega_0 C_{eq,i} \right| \leq \delta_2 \tag{11}$$

Although each layer of meander-line is analyzed separately for both excitations, the computational time is roughly two orders of magnitude lower than the one required for a full wave simulation of the whole ML polarizer. The number of optimization cycles required to achieve the final design of the polarizer directly depends on the number of polarizer sections, but does not depend on the surface of the designed polarizer. The typical number of iterations for the equivalent transmission line circuit optimization is approximately 1000 while the number of iterations for the meander unit cell optimization is around 50. For the designs presented in the next section, the computer time is inferior to 1 hour using a 2.66 GHz quad-core CPU.

4. SYNTHESIZED POLARIZERS

Two Ka-band ML polarizers have been designed following the proposed design procedure. One polarizer has been designed to work for normal incidence ($\theta_{inc} = 0°$), while the second one is optimized for obliquely incident plane waves ($\theta_{inc} = 25°$). Both polarizers are composed of four sections and they are designed to operate in Ka-band (27.5–31.5 GHz). Kapton Polyimide ($\epsilon_r = 3.2$) has been chosen as dielectric substrate because of its thin profile ($l^{(d)} = 100\,\mu\text{m}$) while Rohacell ($\epsilon_r = 1.07$ and variable $l^{(s)}$) has been chosen for the dielectric spacers. The thickness of such substrates has been determined by the availability of this material.

4.1. ML Polarizer Optimized for Normal Incidence ($\theta_{inc} = 0°$)

The dimensions of the polarizer optimized for normal incidence are summarized in Table 1. The magnitude difference ΔM in dB between $\mathbf{E}_{||}$ and $\mathbf{E}_{\perp}$, the differential phase shift $\Delta\Phi$ and the axial ratio AR, corresponding to these dimensions have been computed as function

Table 1. Dimensions of polarizer designed for an incident angle $\theta_{inc} = 0°$.

	Section 1	Section 2	Section 3	Section 4
L_{eq} [nH]	4.89	3.78	3.78	4.89
C_{eq} [fF]	3.52	6.06	6.06	3.52
M_l [mm]	0.970	1.440	1.440	0.970
M_w [mm]	1.480	1.960	1.960	1.480
M_{t1} [mm]	0.195	0.350	0.350	0.195
M_{t2} [mm]	0.140	0.470	0.470	0.140
M_d [mm]	4.385	5.455	5.455	4.385
$l^{(d)}$ [mm]	0.100	0.100	0.100	0.100
$l^{(s)}$ [mm]	1.700	1.350	1.350	1.700

of the frequency using our TL model (Fig. 6). The transmission parameters and the AR are very stable within the band of interest. The AR is lower than 0.4 dB within this band.

4.2. ML Polarizer Optimized for Oblique Incidence ($\boldsymbol{\theta_{inc} = 25°}$)

The dimensions of the polarizer optimized for oblique incidence are summarized in Table 2. Fig. 7 gives the results obtained for the magnitude difference between $\mathbf{E}_{||}$ and $\mathbf{E}_{\perp}$, the differential phase shift $\Delta\Phi$ and the AR as function of the frequency when these dimensions are introduced in our TL model. The transmission parameters and are very stable within the band of interest and the AR is lower than 0.5 dB within this band.

5. PARAMETRIC STUDIES AND TOLERANCE ANALYSIS

The goal of this Section is to show the robustness of the design method. With this purpose, a parametric study has been carried out. This parametric analysis is based on the perturbation of the optimal working condition of the TL model by including the effects on the transmission coefficients of our polarizer of: a) mechanical tolerances, b) non-purity of the linearly polarized field impinging the polarizer and c) non-perfect alignment of the incident field with respect to the meander-line axis. Furthermore, this analysis highlights the main qualitative

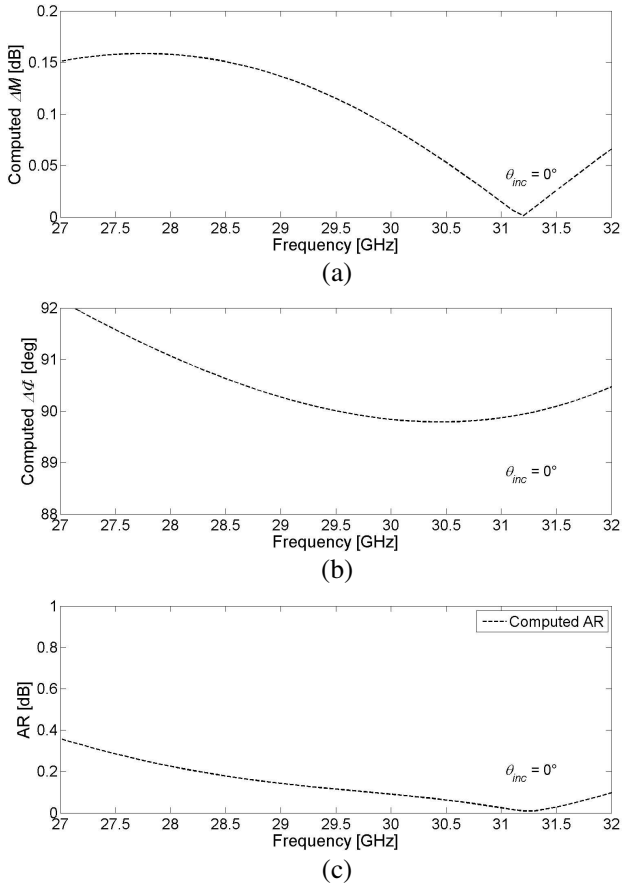

Figure 6. Transmission performances of the synthesized polarizer computed by the equivalent transmission line model for $\theta_{inc} = 0°$. (a) Magnitude difference ΔM. (b) Phase shift $\Delta\Phi$. (c) Axial ratio.

relations between the constitutive parameters of the polarizer and its functionality.

5.1. Effect of Mechanical Tolerances

Here, the tolerances associated to the manufacturing process and the materials used for the assembly of the prototypes have been taken into account. This analysis involves both the unit cell and the TL models. The different dimensions of the meander modeled in the unit cell (Fig. 5) have been perturbed by a tolerance value *TOL*

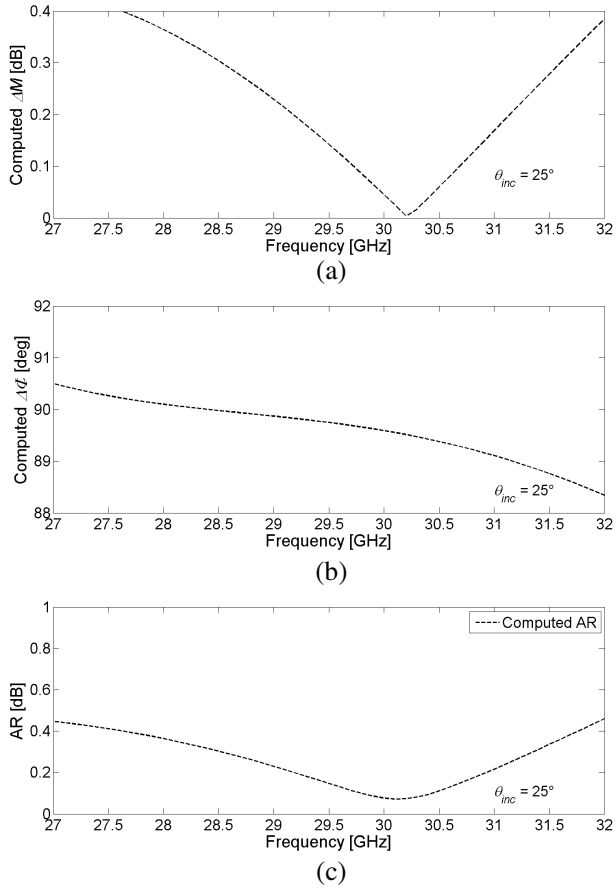

Figure 7. Transmission performances of the synthesized polarizer computed by the equivalent transmission line model for $\theta_{inc} = 25°$. (a) Magnitude difference ΔM. (b) Phase shift $\Delta\Phi$. (c) Axial ratio.

and the relative changes of the admittance have been monitored and included in the TL model. The AR has been computed as described in Section 3.2 for all the possible combinations of tolerance-affected dimensions. This results in a region in the AR vs. frequency diagram which corresponds to the predicted performance degradation of the polarizer due to a given value of the max mechanical tolerance in all the meander dimensions.

For a realistic value of $TOL = \pm 50\,\mu m$, Fig. 8 shows such a tolerance region depicted as a gray area whose lower bound is the computed AR curve when using optimized nominal values for the

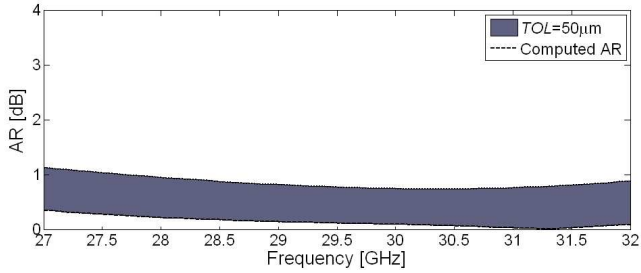

Figure 8. Effect of mechanical tolerances on the axial ratio.

Table 2. Dimensions of polarizer designed for an incident angle $\theta_{inc} = 25°$.

	Section 1	Section 2	Section 3	Section 4
L_{eq} [nH]	8.21	2.57	2.57	7.29
C_{eq} [fF]	5.62	3.37	3.37	5.62
M_l [mm]	1.480	1.480	1.480	1.480
M_w [mm]	2.120	1.390	1.390	2.120
M_{t1} [mm]	0.195	0.350	0.350	0.195
M_{t2} [mm]	0.140	0.465	0.465	0.140
M_d [mm]	8.070	5.300	5.300	7.800
$l^{(d)}$ [mm]	0.100	0.100	0.100	0.100
$l^{(s)}$ [mm]	1.700	1.350	1.350	1.700

meander's dimensions. As it can be easily seen, the worst combination of dimensions with tolerances below 50 μm (upper boundary of the gray area) results in an AR degradation lower than 1 dB in the full frequency band. For the sake of simplicity, Fig. 8 only shows results for normal incidence. A similar degradation has been observed in the prototype optimized for oblique incidence.

5.2. Effect of an Imperfect Linear Polarization of the Impinging Field

Usually, polarizers are designed and optimized assuming a pure linearly polarized incident wave. Obviously, a more realistic scenario must consider an elliptically (quasi-linear) polarized incident wave, that will result in a degradation of the circular polarization emerging after the polarizer.

This effect can be modeled by adding a differential attenuation α_{LP} and a differential phase shift Φ_{LP} to one arm of the TL model, as depicted in Fig. 9. These two parameters are linked to the parallel $\mathbf{E_{0,||}}$ and perpendicular $\mathbf{E_{0,\perp}}$, components of the incident wave field by:

$$\alpha_{LP} = \frac{\left|\mathbf{E_{0,||}}\right|}{\left|\mathbf{E_{0,\perp}}\right|} \tag{12}$$

$$\Phi_{LP} = \angle\mathbf{E_{0,||}} - \angle\mathbf{E_{0,\perp}} \tag{13}$$

and are connected to the axial ratio of the incident wave AR_0 by the expression [23]:

$$\mathrm{AR}_0 = \left(\frac{\alpha_{LP}^2 + 1 + \sqrt{\alpha_{LP}^4 + 2\alpha_{LP}^2\cos\left(2\Phi_{LP}\right) + 1}}{\alpha_{LP}^2 + 1 - \sqrt{\alpha_{LP}^4 + 2\alpha_{LP}^2\cos\left(2\Phi_{LP}\right) + 1}}\right)^{\frac{1}{2}} \tag{14}$$

Now, the scattering parameters of the modified model in Fig. 9 can be easily obtained and from them, the perturbed axial ratio AR of the field after the polarizer can by computed using (9).

As it could be expected, the ML polarizer is quite sensitive to the quality of the linear polarization of the incident wave. Figs. 10 and 11 refer to its performance when designed for normal incidence. For an initial linear polarized wave with AR_0 worse than 35 dB, the circular polarization quality of the wave after the polarizer is unacceptable ($\mathrm{AR} > 3\,\mathrm{dB}$). A similar degradation has been noted in the case of the polarizer optimized for oblique incidence.

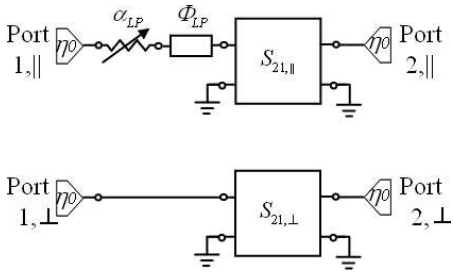

Figure 9. Sensitivity analysis setup scheme. The purity of the linearly polarized incident wave is perturbated by adding a differential attenuation and a differential phase shift to the equivalent model of the polarizer.

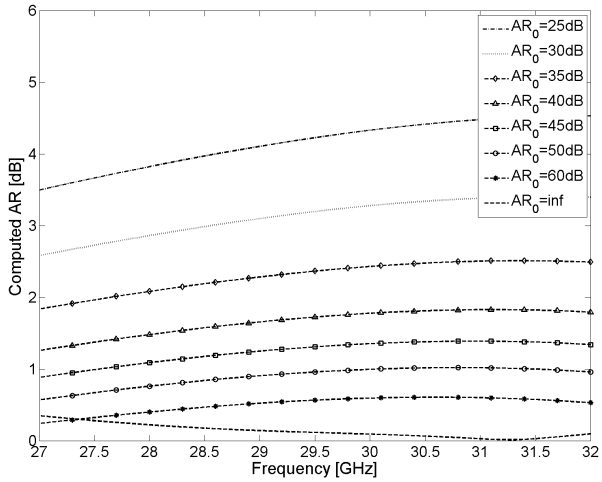

Figure 10. Axial ratio degradation computed for different AR_0.

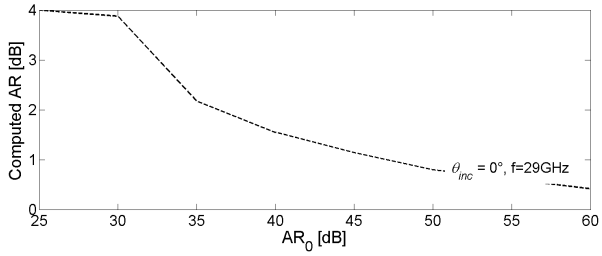

Figure 11. Axial ratio after the polarizer computed for different AR_0 at 29 GHz.

5.3. Effect of Angular Misalignment between the Linear Polarized Wave and the Meander-line Axis

The ML polarizer is obviously optimized for an incident field arriving at an angle $\Psi = 45°$. The effect of an angular misalignment LP of the linear polarized source with the meander-line axis (see Fig. 2(b)) can degrade the polarization of the wave after the polarizer. This effect can be also easily quantified with our TL model by adding a differential attenuation α_{LP} such that:

$$\alpha_{LP} = \frac{\left|\mathbf{E_0}_{,||}\right|}{\left|\mathbf{E_0}_{,\perp}\right|} = \tan\left(\Psi + \Delta\Psi_{LP}\right) \tag{15}$$

The scheme shown in Fig. 9 can be still used maintaining $\Phi_{LP} = 0$ and introducing a value for α_{LP} given by Eq. (15).

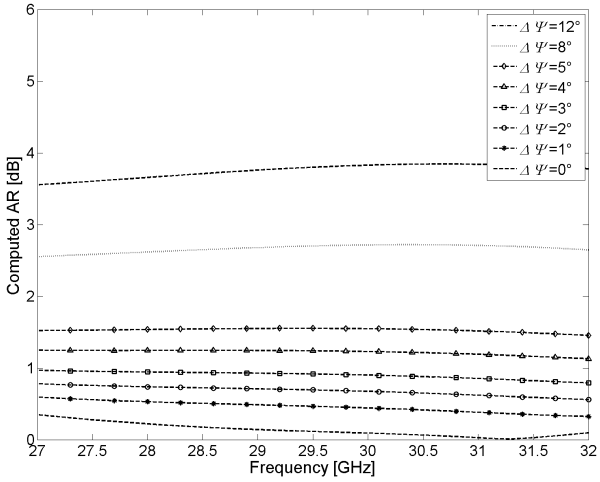

Figure 12. Axial ratio degradation computed for different angular misalignments.

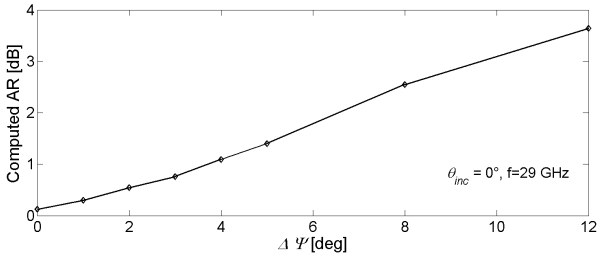

Figure 13. Ratio degradation computed for different angular misalignments at 29 GHz.

Figures 12 and 13 show the effect of the tilt $\Delta\Psi$ on the polarizer optimized for normal incidence. As it can be seen, the degradation is practically frequency independent and amounts approximately to 0.3 dB of AR deterioration for each degree of tilt. The same degradation is noted in the oblique incidence polarizer and when the tilt is directly applied to the linearly polarized horn.

5.4. Generalizing the Sensitivity Analyses

The previous parametric studies show that the proposed model is very well suited to perform a general sensitivity analysis, since it can predict

with very low computational effort the effect of any physical parameter. Moreover, due to the linearity of the used models, the studied three effects and additional ones can be easily combined to predict the sensitivity of the polarizer's performance to any combination of tolerances. This is done in the next section to ascertain the validity of tolerance-prone measurements.

6. PROTOTYPES CHARACTERIZATION

Two ML polarizers have been manufactured (Fig. 14) following the proposed design procedure. Their dimensions are given in Tables 1 and 2. The overall dimensions of the manufactured polarizers are $250 \times 250 \times 6$ mm and the metallization thickness used for realizing the printed meander lines is 0.1 mm.

The performance of the polarizers has been characterized in anechoic chamber, through measurements of the AR using the spinning dipole technique. The antenna subsystem includes a linearly polarizer horn and a 60 mm diameter Teflon lens which generates the linearly polarized plane wave on the polarizer surface [6, 7]. The ML polarizer under test is shown in Fig. 14(c). This measurement setup (see Fig. 15) ensures the test feasibility for beams impinging the polarizer surface within an angle range $-50^\circ \leq \theta_{inc} \leq +50^\circ$.

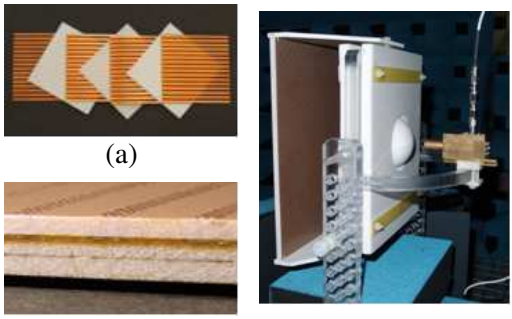

Figure 14. Prototype of (a) meander line polarizer layers and (b) polarizer realization with details of the printed meanders. (c) Measurement setup with polarizer mounted after the lens.

6.1. Measurements of the Polarizer Optimized for Normal Incidence ($\theta_{inc} = 0°$)

Figure 16 compares predicted and measured AR values for the polarizer optimized for normal incidence. In addition to the theoretical AR lower limit, a more realistic predicted range, combining of three possible sources of error ($\Delta\Psi = 1°$, $AR_0 = 45\,dB$ and $TOL = 50\,\mu m$), has been depicted. According to these numerical results, AR should remain around 2 dB within the design frequency band (27–32 GHz). Measurements are sensibly within the region predicted by the model and AR is always better than 3 dB, showing a trend to improve in the upper frequencies.

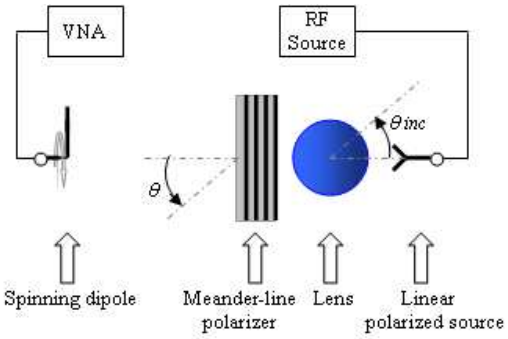

Figure 15. Measurement setup scheme. A plane wave is created by illuminating a dielectric homogeneous Teflon lens with a linearly polarized horn. The polarizer changes the polarization of the lens outgoing wave. The polarization quality is measured by spinning dipole technique in the anechoic chamber.

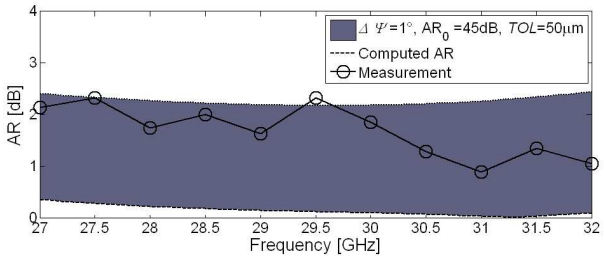

Figure 16. Axial ratio computed for $\Delta\Psi = 1°$, $AR_0 = 45\,dB$. The region in gray includes the performances degradation due to mechanical tolerances.

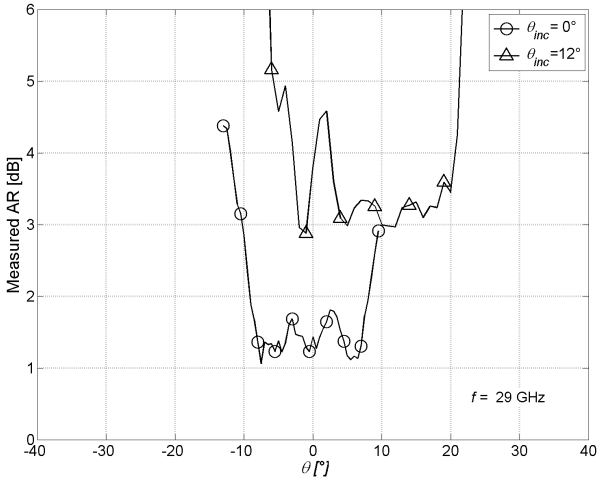

Figure 17. Measured axial ratio of meander-line polarizer designed for normally incident plane wave. The direction of the incoming wave is $\theta_{inc} = 0°$ and $\theta_{inc} = 12°$.

The AR has been also measured for two different incident angles ($\theta_{inc} = 0°$ and $12°$) as function of the polar angle θ at frequency $f_0 = 29\,\text{GHz}$. Fig. 17 shows that for normal incidence, the AR remains better than 2 dB within the range $-12° \leq \theta - \theta_{inc} \leq +12°$. For a higher incidence angle ($\theta_{inc} \geq 12°$) the AR still remains centered around the broadside direction $\theta = \theta_{inc}$ but its average value is higher (slightly above 3 dB) and also deteriorates quickly outside the range $-12° \leq \theta - \theta_{inc} \leq +12°$.

Indeed, a study at a fixed frequency $f_0 = 29\,\text{GHz}$ and in the broadside direction ($\theta = \theta_{inc}$) as a function of the planar-wave incident angle θ_{inc}, is given in Fig. 18. The measured polarization quality is very good for normal incidence ($\theta_{inc} = 0°$) but deteriorates quickly when the incident angle θ_{inc} increases. The AR crosses the 3 dB line at around $\theta_{inc} = 12°$. This shows clearly the need to redesign the polarizer for specific oblique incidence angles.

6.2. Measurements of the Polarizer Optimized for Oblique Incidence ($\theta_{inc} = 25°$)

When the polarizer is specifically designed for an oblique incidence angle, a measured value of the AR lower than 3 dB is recovered within the full 28–31.5 GHz band (Fig. 19). Again, the measured

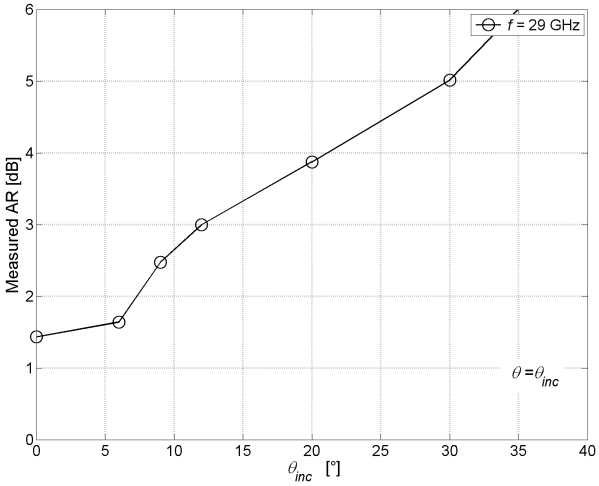

Figure 18. Measured axial ratio of the meander-line polarizer designed for normally incident plane wave. The performances of the polarization quality degrade increasing θ_{inc}. The axial ratio becomes unacceptable for $\theta_{inc} > 12^\circ$ and this justifies the design of a different polarizer for obliquely incident plane wave.

values are within the tolerance range corresponding to the combination ($\Delta\Psi = 1^\circ$, $\mathrm{AR}_0 = 45\,\mathrm{dB}$ and $TOL = 50\,\mu\mathrm{m}$).

In Fig. 20, the AR has been measured for different incident angles ($0^\circ \leq \theta_{inc} \leq 40^\circ$) at two different frequencies, 29 and 31 GHz. The AR behavior remains centered broadside and acceptable in the range of $-12^\circ \leq \theta - \theta_{inc} \leq +12^\circ$.

In Fig. 21, the planar-wave incident angle θ_{inc} is varied, while keeping the measurements in the broadside direction ($\theta = \theta_{inc}$). The incidence angle sweep is done at two frequencies 29 and 31 GHz. Results show that the oblique design is clearly successful, allowing to improve the AR performances for a large range of oblique incident angles ($12^\circ \leq \theta_{inc} \leq 30^\circ$), while showing only a very minor reduction of the frequency band (28–31.5 GHz). This validates the proposed one-step design procedure even though additional improvements are still possible through fine tuning and further iterations.

6.3. Simulations Versus Measurements

It is expected that an even better agreement between the computed and the measured AR could be obtained if several improvements are

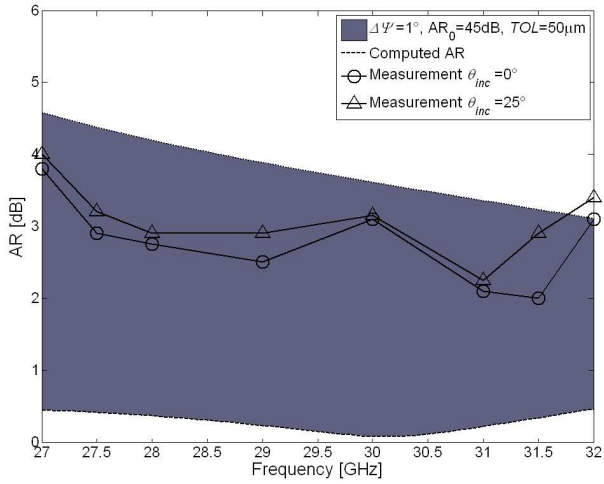

Figure 19. Axial ratio computed for $\Delta\Psi = 1°$, $\mathrm{AR}_0 = 45\,\mathrm{dB}$. The region in gray includes the performances degradation due to mechanical tolerances.

introduced in both the mathematical model and the measurement procedures. On the modeling side, the obvious improvements would be:

- The meander-lines are assumed to be infinitely thin in the TL model. This typically produces a frequency shift of the predicted electrical response [25].
- The mutual coupling between the $\mathbf{E}_{||}$ and $\mathbf{E}_{\perp}$ components into the polarizer has not been included in the TL model. For waves with oblique incident angle, this coupling effect is more pronounced.
- The presence of higher order modes between the polarizer layers has not been included in this analysis. Although those modes are evanescent, they contribute to increase the insertion losses differently for the $\mathbf{E}_{||}$ and $\mathbf{E}_{\perp}$ components, influencing the performances of the whole polarizer. For waves with oblique incident angle, this effect is more pronounced.
- Obviously, more accurate results could be obtained if a full wave model is used, including coupling between parallel and perpendicular polarizations and the effect of higher order modes. However, computer time for complete analysis using full-wave models is prohibitive and partial implementation done at normal incidence shows no significant change from TL predictions.

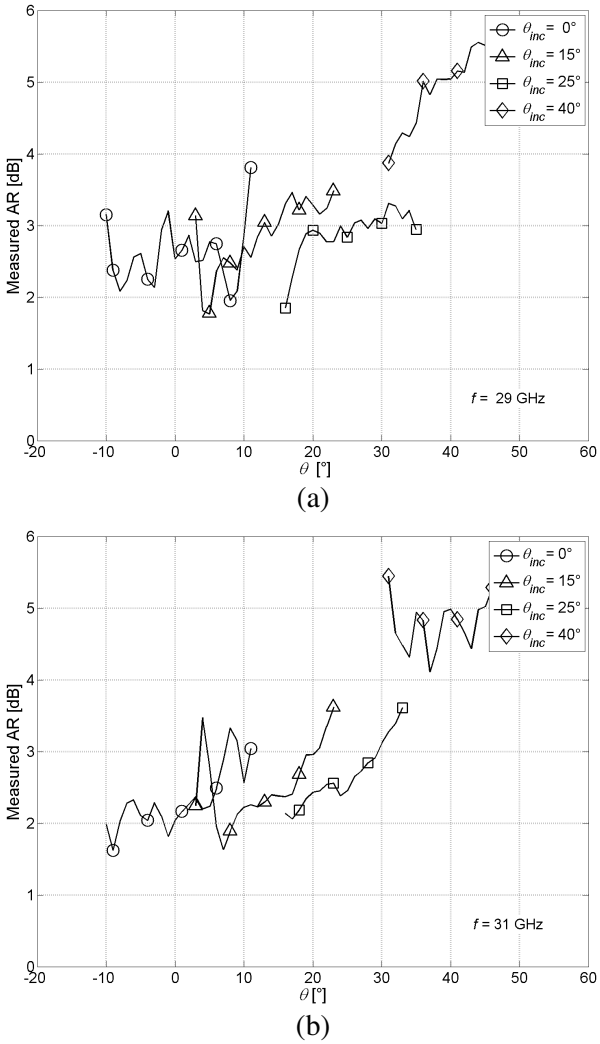

Figure 20. Measured axial ratio of meander-line polarizer designed for obliquely incident plane wave. The polarizer works for oblique angles of incidence. (a) At 29 GHz. (b) 31 GHz.

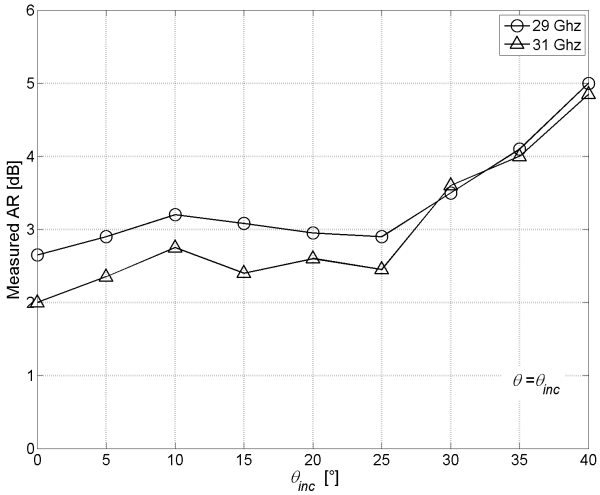

Figure 21. Measured axial ratio of meander-line polarizer designed for obliquely incident plane wave. The axial ratio becomes unacceptable for $\theta_{inc} > 30°$.

Moreover the dispersion due to tolerances as shown in Figs. 16 and 19 is certainly larger than the discrepancies between the two model.

Measurements could be also improved if the following effects are mitigated or fully eliminated:

- The ML polarizer surface is not infinite and the effect of the plated edges impacts on the quality of the measured AR.
- The incident wave on the ML polarizer is not uniform. A homogeneous Teflon lens ($\oslash = 60\,\text{mm} \approx 6\lambda_0$) is used to generate the plane wave and its measured gain is 20 dB in Ka-band. A higher gain lens might improve the uniformity of the plane wave impinging into the polarizer. Furthermore, the quality of the plane wave is influenced by the distance between lens and polarizer. Ideally, the polarizer should be in the lens far-field. But it must be close enough to be seen by the lens as having very large transverse dimensions and reduce diffraction edge effect. So in practice a trade off has to be made.
- The manufacturing tolerances of the prototyped polarizer and the undesired misalignments between horn, lens, polarizer and receiver should be reduced as much as possible.

7. CONCLUSIONS

This paper has presented a method based on a TL model and a full wave unit-cell analysis for the design of ML polarizers operating with waves impinging on its surface with its incident field θ_{inc} parallel to the polarizer surface and at an arbitrary oblique incidence angle. This is a situation currently encountered in lens antenna subsystems and the design of the polarizer has been demonstrated by two prototypes working in Ka-band.

One prototype has been optimized for normal incidence. The AR is lower than 3 dB within the measured frequencies band and within the range of $-12^\circ \leq \theta \leq +12^\circ$. However, the AR degrades, when the incident angle θ_{inc} increases and it is higher than 3 dB for $\theta_{inc} \geq 12^\circ$. A second prototype has been optimized for waves impinging on its surface obliquely with an incident angle $\theta_{inc} = 25^\circ$. The frequency band of this polarizer is (28–31.5 GHz), whereas its circular polarization quality, on average, is not as good as the one designed for normal incidence but this polarizer can be used for plane wave impinging its surface with a broader angle range (within $0^\circ \leq \theta_{inc} \leq 30^\circ$).

The design procedure has been validated with measured data and, besides reducing significantly the development cycle, it has also introduced the possibility of designing ML polarizers for plane waves impinging its surface obliquely. Sensitivity analysis has been introduced in this work to give a quantitative insight on the effect of any tolerance on the optimal working condition of the polarizers.

ACKNOWLEDGMENT

This research has been initiated within the European COST Action IC0603 "ASSIST" and IC1102 "VISTA" and performed thanks to the financial support of the Swiss CTI Project 126371 "CHAPS". The authors also wish to thank the StratXX staff, partners in the CTI project, for helpful discussions and support, as well as the EPFL Workshops for the careful realization prototypes.

REFERENCES

1. Qu, Y., G. S. Liao, S. Q. Zhu, and X. Y. Liu, "Pattern synthesis of planar antenna array via convex optimization for airbone forward looking radar," *Progress In Electromagnetics Research*, Vol. 84, 1–10, 2008.
2. Costa, F., A. Monarchio, "Design of subwavelength tunable

and steerable fabry-perot/leaky wave antennas," *Progress in Electromagnetics Research*, Vol. 111, 467–481, 2011.

3. Exposito-Dominguez, G., J. M. Fernandez-Gonzalez, P. Padilla de la Torre, and M. Sierra-Castner, "Dual circular polarized steering antenna for satellite communications in X band," *Progress In Electromagnetics Research*, Vol. 122, 61–76, 2012.
4. Dessouky, M., H. Sharshar, and Y. Albagory, "Design of high altitude platforms cellular communications," *Progress In Electromagnetics Research*, Vol. 67, 251–261, 2007.
5. Peebles, A. L., "A dielectric bifocal lens for multibeam antenna applications," *IEEE Transactions on Antennas and Propagation*, Vol. 36, 599–606, 1988.
6. Letizia, M., B. Fuchs, A. Skrivervik, and J. R. Mosig, "Circularly polarized lens antenna system providing multibeam radiation pattern for HAPS," *Radio Science Bulletin*, No. 330, 18–28, Mar. 2010.
7. Letizia, M., J.-F. Zürcher, B. Fuchs, J. R. Mosig, and A. Skrivervik, "Circularly polarized multi-beam lens antenna system for high altitude platforms (HAPS)," *EuCAP 2011, 5th European Conference on Antennas and Propagation*, 1051–1055, 2011.
8. Zürcher, J. F., "A meander-line polarizer covering the full E-band (60–90 GHz)," *Microwave Opt. Technol. Lett.*, Vol. 18, 320–323, Aug. 1998.
9. Young, L., L. A. Robinson, and C. A. Hacking, "Circularly polarized lens antenna system providing multibeam radiation pattern for HAPS," *IEEE Transactions on Antennas and Propagation*, Vol. 21, 376–378, May 1973.
10. Marino, R. A., "Accurate and efficient modeling of meanderline polarizers," *Microw. J.*, Vol. 41, No. 11, 22–34, Nov. 1998.
11. Epis, J. J., "Broadband antenna polarizers," US Patent 3754271, Aug. 1973.
12. Blackney, T. L., J. R. Burnett, and S. B. Cohn, "A design method for meander-line circular polarizers," *22nd Ann. Antenna Symp.*, 1–5, Oct. 1972.
13. Terret, C., J. R. Level, and K. Mahdjoubi, "Susceptance computation of a meander-line polarizer layer," *IEEE Transactions on Antennas and Propagation*, Vol. 21, 1007–1011, Sep. 1984.
14. Lee, S. W. and G. Zarrilo, "Simple formulas for transmission through periodic metal grids or plates," *1983 Antenna Application*

Sym., University of Illinois, Urbana, IL, Sponsored by RADC (EEA) Electromagnetic Sciences Division, Hanscom AFB, 1983.

15. Bhattacharyya, A. K. and T. J. Chwalek, "Analysis of multilayered meander line polarizer," *Int. J. of Microwave and Millimeter-wave Computer-aided Eng.*, 442–454, 1997.
16. Joyal, M.-A. and J.-J. Laurin, "Analysis and design of thin circular polarizers based on meander lines," *IEEE Transactions on Antennas and Propagation*, Vol. 60, 3007–3011, Sep. 2012.
17. Chen, C. C., "Scattering by a two-dimensional periodic array of conducting plates," *IEEE Transactions on Antennas and Propagation*, Vol. 18, 660–665, May 1970.
18. Chu, R. S. and K. M. Lee, "Radiation impedance of a dipole printed on periodic dielectric slabs protruding over a ground plane in an infinite phased array," *IEEE Transactions on Antennas and Propagation*, Vol. 35, 13–25, Jan. 1987.
19. Chu, R. S. and K. M. Lee, "Analytical model of a multilayered meander line polarizer plate with normal and oblique plane-wave incidence," *IEEE Transactions on Antennas and Propagation*, Vol. 35, 652–661, Jun. 1987.
20. Munk, B. A., *Finite Antenna Arrays and FSS* , 306–326, John Wiley and Sons, 2003.
21. Marcuvitz, N., *Waveguide Handbook*, Radiation Laboratories Series, 28–33, 280–289, McGraw-Hill Book Co., Inc., New York, NY, 1951.
22. Pozar, D. M., *Microwave Engineering*, 2nd Edition, 29–49, 208–211, John Wiley and Sons, New York, 1998.
23. Balanis, C. A., *Antenna Theory*, 2nd Edition, 66–68, John Wiley and Sons, New York, 1997.
24. www.ansoft.com.
25. Chan, K. K., T. W. Ang, T. H. Chio, and T. S. Yeo, "Accurate analysis of meanderline polarizers with finite thicknesses using mode matching," *IEEE Transactions on Antennas and Propagation*, Vol. 56, 3580–3585, Nov. 2008.